www.vbripress.com/aml, DOI: 10.5185/amlett.2016.5974 Published online by the VBRI Press in 2016

Synthesis, characterization and investigation of visible light photocatalytic activity of C, N co-doped ZnO

Atul B. Lavand, Yuvraj S. Malghe*

Department of Chemistry, The Institute of Science, Mumbai 400032, India

*Corresponding author. Tel: (+91) 22-22844219; Fax: (+91) 22-22816750; E-mail: ymalghe@yahoo.com

Received: 04 May 2015, Revised: 03 December 2015 and Accepted: 03 January 2016

ABSTRACT

Nanosized bare, C and N doped as well as C, N co-doped ZnO nanopowders were prepared using microemulsion method. Synthesized powders were characterized using X-ray diffraction(XRD), Fourier transform infrared spectrophotometer (FTIR), scanning electron microscope (SEM), energy dispersive X-ray spectroscopy (EDX), CHNS analyzer, photoluminescence spectrophotometer and UV-visible spectrophotometer. XRD study shows that C, N co-doped ZnO have hexagonal wurtzite structure. UV-visible spectral study reveals that C and N co-doping improves photo absorption capacity in visible region. Visible light photocatalytic degradation of malachite green was carried out using nanosized bare, C doped and C, N co-doped ZnO. C, N co-doped ZnO exhibits better visible light photocatalytic activity as compared to pure and C doped ZnO. Also the photocatalyst prepared is stable and can be reused repeatedly. Copyright © 2016 VBRI Press.

Keywords: Visible light; photocatalysis; C, N co-doped ZnO; microemulsion; malachite green.

Introduction

Malachite green (MG) is extensively used biocide in aquaculture industry, and shows excellent antifungal and anti-protozoa activity. Millions of kilograms of MG and related triarylmethane dyes are produced annually for this purpose. It is also used as food coloring agent, food additive, anthelminthic and as a medical disinfectant. It is used for dying wool, silk, leather, cotton, jute, paper etc. **[1-4]**. However, it became highly controversial compound due to its effects on human immune and reproductive system through treated fish. It is risky to use this compound due to its carcinogenic and genotoxic properties. The presence of MG in water causes considerable damage to the aquatic environment as well as human beings or other animals coming in the contact of infected fish. It is necessary to remove this compound from water. Photocatalysis is one of the promising and effective methods used for degradation of organic compounds/dyes **[5, 6]**. This process involves the acceleration of photoreaction in presence of semiconductor photocatalyst. When a photocatalyst is illuminated by light with energy equal to or greater than its band-gap energy, the valence band electrons get excited to the conduction band, leaving a positive hole in the valence band.

$$ZnO \xrightarrow{h\nu} e^{-}_{CB} + h^{+}_{VB}$$

The excited electron-hole pairs recombine, releasing the energy as heat, with no chemical effect. However, if the electrons (and holes) migrate to the surface of the semiconductor without recombination, they can participate in various oxidation and reduction reactions with adsorbed species such as water, oxygen, and other organic or inorganic species. These oxidation and reduction are basic reactions involved in photocatalytic degradation of pollutants present in water/air. TiO_2 is well known photocatalyst and widely used for waste water treatment **[7-12]**. Daneshvar *et al.* **[13]** reported that ZnO can be used as suitable alternative to TiO_2 since its photodegradation mechanism is similar to that of TiO_2. In the past two decades, ZnO has attracted much attention and used as photocatalyst due to its high photosensitivity, non-toxic nature, stability and wide band gap **[14, 15]**. Zinc oxide is thought as a low cost alternative to TiO_2 photocatalyst for degradation of organic pollutants present in water **[16]**. Main advantage of ZnO is that it absorbs a larger fraction of the solar spectrum as compared to TiO_2 hence considered more suitable for photocatalytic degradation in presence of sunlight **[17, 18]**. ZnO has a large band gap (3.37eV) and its application in photocatalysis is limited to UV light only **[19-22]**. It has other certain disadvantages like instability in acidic conditions, and low surface area of the bulk form. It is known that photocatalytic activity of ZnO depends on size of particles. The larger the size of ZnO particles higher is the rate of electron-hole pair recombination at or near its surface, resulting in lower photocatalytic activity. To conquer these drawbacks nanosized ZnO is used as photocatalyst. Due to quantum confinement of nanostructured materials, the separation rate of charge carriers in semiconductor photocatalyst can be significantly increased by reducing its size to nano level

and enhance its quantum efficiency and photocatalytic activity. To improve the photocatalytic activity of ZnO further, various efforts have been made, which includes surface modification, semiconductor coupling, doping with a heteroatom in place of Zn/O atom. Among these methods, doping is one of the efficient methods to improve its photocatalytic activity. It is reported that N/C doping significantly increases the photocatalytic activity of metal oxide in visible light **[23- 26]**. However, only few reports are available on C and N doped ZnO. Therefore in the present work we have synthesized bare, C and N doped as well as C, N-co-doped ZnO nanostructures using microemulsion method. The major advantages of this method are low reaction temperature, short processing time, and control of morphology, the attractive effect of preventing agglomeration in the nanoparticles formed and nanoparticles prepared are homogeneous. Also, the visible light photocatalytic activities of synthesized nanomaterials were investigated for the degradation of MG.

Experimental

Materials

Malachite green (MG) (bis[p-dimethylaminophenyl] phenyl-methylium oxalate) used in the present study was purchased from Merck Chemicals, Mumbai and used without any further purification. Zinc nitrate hexahydrate ($Zn(NO_3)_2.6H_2O$), Guanidine nitrate ($CH_6N_4O_3$), cyclohexane, n-butanol, N,N,N-cetyl trimethyl ammonium bromide (CTAB), acetone, sodium hydroxide (NaOH) and ethanol used for the synthesis are AR grade. All these chemicals were procured from SD Fine Chemicals, Mumbai and used without further purification.

Synthesis of pure and doped ZnO

1M solution of zinc nitrate was prepared by dissolving 29.74g of $Zn(NO_3)_2$. $6H_2O$ in 100 mL distilled water. 2M sodium hydroxide solution was prepared by dissolving 8g NaOH in 100 mL distilled water. To 28.8mL 1M zinc nitrate, 2g guanidine nitrate, 35.5 mL cyclohexane, 8 mL butanol and 5.90g CTAB were added. In another solution 28.8mL 2M NaOH, 35.5mL cyclohexane, 8mL butanol and 5.90g CTAB were mixed. Both these solutions were stirred continuously with the help of magnetic stirrer to form clear solutions. These clear solutions were mixed with each other. The mixture was transferred to teflon lined autoclave and heated in an oven at 150 °C for 1h. After, autoclave was cooled to room temperature. The solid product formed was separated by filtration, washed with distilled water followed by ethanol and finally with acetone and dried in an oven at 60 °C. Hydrothermal product thus obtained was characterized using various characterization techniques. C, N co-doped and N doped ZnO powders were prepared by heating the hydrothermal product (precursor) at 300 and 500 °C for 2h. C doped and pure ZnO powders were prepared by same method. During this preparation guanidine nitrate (source of N) was not added in first solution. Hydrothermal product (precursor) thus obtained was calcined at 300 and 500 ^{0}C for 2h yielded C doped and pure ZnO respectively.

Characterization

TG and DTA curves of precursor were recorded using simultaneous TG/DTA recording system (Rigaku, Model-Thermo Plus TG8120). For recording TG and DTA curves 10.18 mg precursor was heated in a nitrogen atmosphere upto 300 °C and after in static air with a constant heating rate 10 °Cmin^{-1}. For recording DTA curve, alumina was used as a reference material. FTIR spectra of precursor and the precursor calcined at 300, 400 and 500 ^{o}C were recorded using FTIR spectrophotometer (Perkin-Elmer). Precursor samples were calcined at 300, 400 and 500 ^{o}C for 2h and the XRD patterns of the product obtained at different temperatures were recorded using X-ray diffractometer (Rigaku, Model-Miniflex II) using monochromatized CuKα radiation (λ= 0.15405 nm) with scanning rate 2° 2θ min^{-1}. Qualitative elemental analysis was carried out using energy dispersive X-ray spectroscopy (EDX) (JEOL- JSM6360A) technique. Band gap energies of synthesized nano powders were evaluated from UV visible spectra recorded using UV visible spectrophotometer (Shimadzu, Model-1800). Photoluminescence spectra of samples were recorded at room temperature using Fluorescence spectrophotometer (Perkin Elmer- LS-55) with excitation wavelength 350 nm.

Photocatalytic activity study

Photocatalytic activities of pure and doped ZnO were investigated for degradation of MG solution. Reaction suspension was prepared by adding 0.05g pure/ doped ZnO photocatalyst in 100 mL, 10 ppm MG solution. This aqueous suspension was stirred in the dark for 30 min to attain adsorption-desorption equilibrium. Later, the solution was irradiated with visible light. The visible light irradiation was carried out in a photo reactor using a compact fluorescent lamp (65W, λ >420nm, Philips). Intensity of the light reaching to the test solution is 42W/m^2. Temperature of test solution was maintained constant throughout the experiment by circulating water around the solution. The amount of MG was monitored by sampling out 5 ml of aliquot solution at regular time intervals. The catalyst was separated by centrifugation and the concentrations of MG in the supernatant solution were estimated using UV-visible spectra recorded in the wavelength range 200-800 nm.

Results and discussion

TG and DTA study

Simultaneous TG and DTA curves recorded for thermal decomposition of precursor are presented in **Fig. 1**. TG curve shows that there is gradual weight loss from 25-300 ^{o}C, this could be attributed to vaporization of absorbed water molecules, cyclohexane and burning of residual surfactant. Also, this change is observed in DTA curve as endothermic peaks in the same temperature range with minima located near 104 and 201 ^{o}C. Above 300 ^{o}C there is slight decrease in mass in presence of static air accompanied with exothermic peak near 385 °C, which is due to C content in the sample and mass loss is found to be 3.69 wt %. No mass loss is observed above 400 ^{o}C and TG

curve gives a straight line. It indicates that precursor yields stable product above 400 °C.

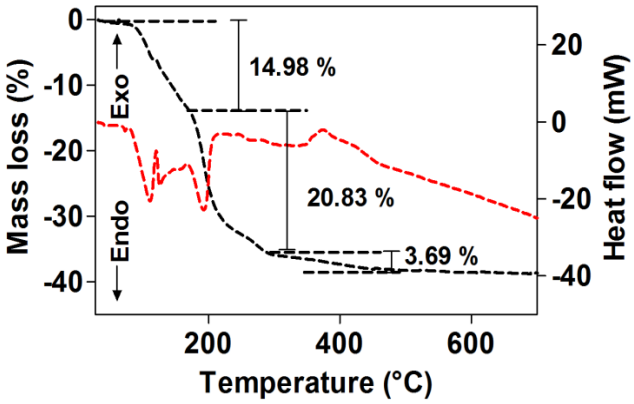

Fig. 1. TG and DTA curves of precursor (recorded in nitrogen + air).

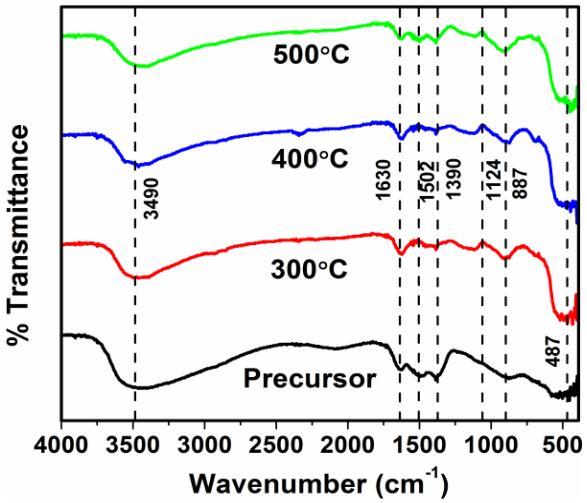

Fig. 2. FTIR spectra of precursor and precursor calcined at different temperatures.

FTIR study

FTIR spectra of precursor and product obtained after calcination of precursor at different temperatures for 2 h are presented in **Fig. 2**. Precursor shows absorption peaks at 3490 and 1630 cm^{-1} which corresponds to the O–H stretching and bending vibration of the –OH bond **[27]**. Peak at 1124 cm^{-1} can be assigned to C-O stretching in carbonyl. Two peaks at 1390 and 1502 cm^{-1} may correspond to the vibration of the Zn–N bonds **[28]**, represents successful doping of N. These spectra show absorption peaks below 600 cm^{-1} which corresponds to the characteristic absorption of Zn-O bond in zinc oxide **[29]**. FTIR spectra of product obtained after heating the sample at 300, 400 and 500 °C for 2h shows that peak corresponds to –OH vibrational modes became less intense and gives the sharp peak below 500 cm^{-1} which may be due to stretching frequency of Zn-O bond in zinc oxide. It is observed that as calcination temperature increases from 300 to 500 °C, Zn-O stretching vibration frequency shifts from 487 to 436 cm^{-1}. This may be due to change in morphology of the sample and alteration of two element doping to single element doping with increase in temperature.

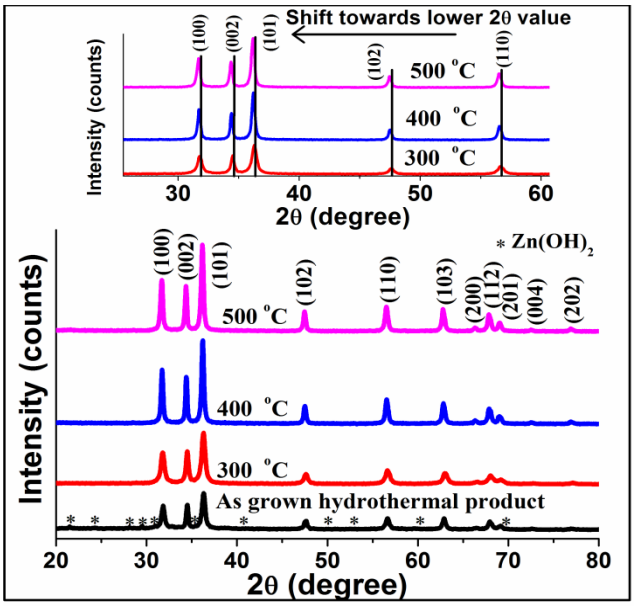

Fig. 3. XRD patterns of precursor, precursor calcined at different temperatures and inset shows expanded view.

XRD study

Fig. 3 shows XRD patterns of the precursor and product obtained after heating precursor at 300, 400 and 500 °C. XRD pattern of precursor sample shows peaks corresponds to hexagonal wurtzite ZnO along with small peaks corresponds to $Zn(OH)_2$ (JCPDS 712215). These patterns suggest that product obtained by heating the sample at different temperatures is crystalline in nature and is in good agreement with the wurtzite ZnO phase (JCPDS 36-1451). No other peaks correspond to C and N is observed which implies that O is substituted by C and N without affecting crystal structure of ZnO **[30]**. Slight shift toward lower 2θ value with increasing calcinations temperature (inset of **Fig. 3**) is observed. This may be due to the fact that product obtained at 300 and 400 °C contains C and N whereas product obtained at 500 °C contains only N. Considerable peak broadening and decrease in crystallinity is observed as compared to pure ZnO, which demonstrates that C and N are successfully incorporated in ZnO lattice. Effect of doping on lattice parameters a and c of ZnO with respect to calcination temperature is shown in **Fig. S1** and corresponding parameters are presented in **Table 1**. The intensity peak ratios of (002)/(101) planes are different from that of the standard ZnO (JCPDS) peak ratios, which indicates that ZnO has preferential growth direction. From the c/a ratio, it is contingent that ZnO prepared at 400 °C has c-axial growth. Crystallite size and lattice strain induced due to broadening are determined using Williamson-Hall (W-H) equation **[31],**

$$\frac{\beta Cos\theta}{\lambda} = \frac{1}{D} + \frac{4\,\varepsilon\, Sin\theta}{\lambda}$$

where, β is the full width at half maximum (FWHM), θ is diffraction angle, λ is X-ray wavelength, D is crystallite size and ε is lattice strain. Graph of $\frac{\beta Cos\theta}{\lambda}$ versus $\frac{4\ Sin\theta}{\lambda}$ was plotted to obtain strain and crystallite size from slope

and intercept of linear fit. **Fig. 4** illustrates W-H plot and effect of lattice strain with respect to temperature for ZnO samples. Positive slope indicates that tensile strain is consistent with the lattice expansion. Slopes of the plots provides the values of strain (ε) which are 0.00295, 0.00168 and 0.0011 for the samples calcined at 300 °C, 400 °C and 500 °C. It is observed from the calculation that with increase in temperature from 300 °C to 500 °C, the strain associated with the samples decreased as shown in **Table 1**. Average crystallite size and strain calculated from W-H plot for each sample is presented in **Table 1**. Sample prepared at 300 °C display highest lattice strain whereas sample prepared at 500 °C has the lowest strain. This is because sample prepared at 300 and 400 °C contains doped C and N.

Table 1. Characteristic properties of photocatalyst.

Sample	Calcination Temperature	Lattice parameters				Crystallite size (nm)	Strain	Intensity ratio (002/101)	Band gap (eV)
		a=b (A^0)	c (A^0)	c/a	V (A^{03})				
C, N co-doped ZnO	300°C	3.250	5.207	1.6021	54.99	28.89	0.00295	0.653	2.16
C, N co-doped ZnO	400°C	3.252	5.212	1.6027	55.12	37.77	0.00168	0.569	2.28
N doped ZnO	500°C	3.249	5.205	1.6019	54.95	26.31	0.00110	0.517	2.40

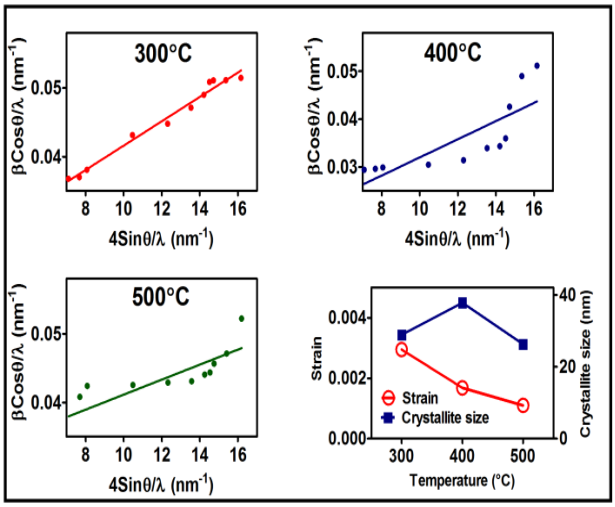

Fig. 4. Williamson-Hall (W-H) plot for ZnO samples and variation of lattice strain and crystallite size with respect to temperature.

CHNS analysis

Amount of C and N present in the precursor heated at different temperatures were obtained from CHNS analysis. CHNS analysis data reveals that precursor heated at 300 °C for 2 h contains 2.29 and 3.61 % C and N respectively. Product obtained at 400 °C contains 0.62 and 3.58 % C and N and the product obtained at 500°C contains only 3.50 % N.

FE-SEM study

FE-SEM micrographs of precursor heated at different temperatures were recorded and are presented in **Fig. 5(a)** to **(c)**. It shows that C, N co-doped ZnO prepared at 300 °C is having rod like shape **(Fig. 5(a))**. At 400 °C this rod shape initiated to transform into spherical shape and therefore it shows mixture of rods and spheres **(Fig. 5(b))**. However, N doped ZnO particles obtained at 500 °C are mostly spherical in shape **(Fig. 5(c))**. Elemental composition of precursor heated at 300, 400 and 500 °C was obtained from energy dispersive X-ray (EDX) spectra **(Fig. S2).**

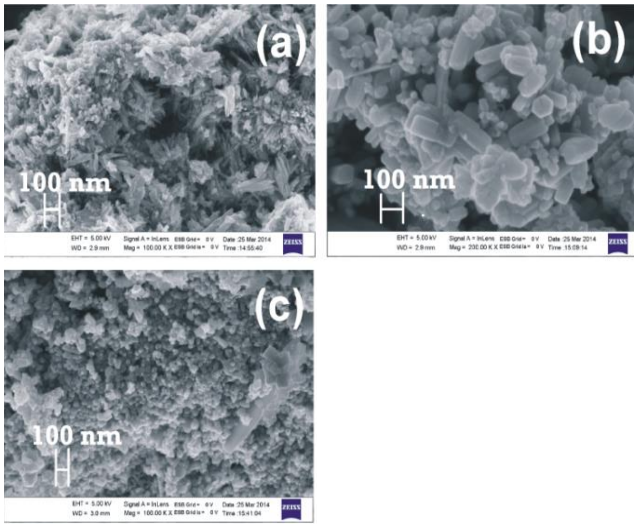

Fig. 5. FE-SEM images of precursor calcined at (a) 300, (b) 400 and (c) 500 °C.

After careful evaluation of the above results, the over-all mechanism of formation of C/N-doped ZnO by the microemulsion route can be visualized as shown in **Fig. S3**. If microemulsions containing $Zn(NO)_3$ and guanidine nitrate are heated at 150 °C in an autoclave, $Zn(NO)_3$ based Zn–guanidine nitrate nuclei get formed. Oxley *et al.* **[32]** proposed possible decomposition routes of guanidine nitrate and reported that guanidine nitrate dissociates and gives nitric acid and NH_3. In present case precursor obtained is the mixture of $Zn(OH)_2$, NH_3 and ZnO. After calcining this precursor at different temperatures we got nanorods (at 300 °C), mixture of nanorods and nanospheres (at 400 °C) and nanospheres (at 500 °C). Product obtained at 300 and 400 °C consists C. At high temperature C get evaporated hence precursor heated at 500 °C does not contain C. Change in morphology of the sample with respect to calcination temperature is mainly due to presence of $Zn(OH)_2$ in the precursor. **Fig. S4** represents the XRD pattern of ZnO precursor. It clearly indicates the presence of $Zn(OH)_2$ and ZnO. FTIR spectra (inset **Fig. S4**) of precursor also confirms the presence of Zn-O and (-OH) groups.

Band gap study

The absorption properties of pure/C doped ZnO and N containing precursor calcined at 300, 400 and 500 °C were investigated from their UV−visible spectra **(Fig. 6(A))**. Pure ZnO is white in color and have an absorption cut off edge at 395 nm, corresponding to a band gap 3.08 eV. C doped ZnO is brown in color and gives absorption edge at 425nm corresponds to a band gap 2.69eV. C, N co-doped ZnO samples obtained at 300 and 400 °C (pale yellow color) exhibits strong and broad absorption band in the wavelength range 440 to 650 nm. N doped ZnO

obtained at 500 °C is light yellow in color and have an absorption cut off edge at 475 nm. It is recommended that the N doping allows sub-band-gap excitation which is due to an isolated N_{2p} state rather than mixed states of N_{2p} and O_{2p} **[33, 34]**. More light reaching at the surface of the C, N-doped ZnO photocatalyst is absorbed due to the introduction of the doping structures, which results in multiple reflections of the incident light during irradiation. This study reveals that C and N doping shows remarkable influence in absorption characteristics and electronic structure of ZnO. Tauc plot **(Fig. 6 (B))** shows that with doping the band gap energy of ZnO reduced from 3.08 to 2.16 eV.

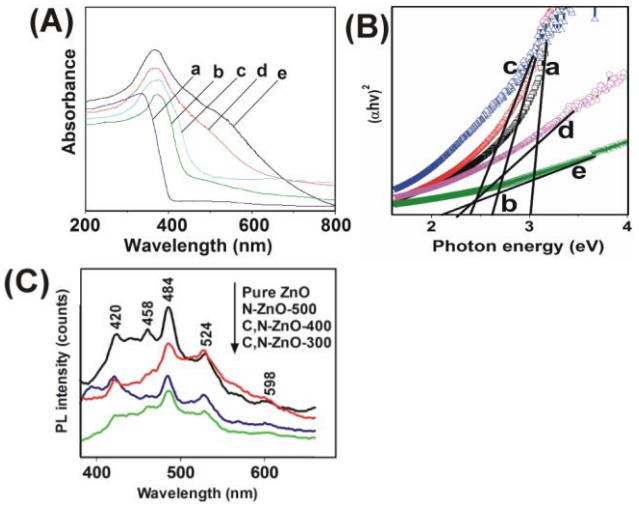

Fig. 6. (A) UV-visible absorption spectra of (a) pure ZnO, (b) C doped ZnO and precursor calcined at (c) 500, (d) 400, (e) 300 °C, **(B)** Tauc plots, $(\alpha h\nu)^2$ versus photon energy (eV) of (a) pure ZnO, (b) C doped ZnO and precursor calcined at (c) 500, (d) 400, (e) 300 °C and **(C)** Photoluminescence spectra as a function of wavelength for (a) pure ZnO, and precursor calcined at (b) 500, (c) 400, (d) 300 °C.

Photoluminescence study

Photoluminescence (PL) measurements were carried out using pure and doped ZnO samples. PL spectra were recorded and are presented in **Fig. 6 (C)**. Four sharp bands are observed in the visible region which indicates that PL emission is due to deep level introduced by defect or by trap state. PL emission band at 420 nm is due to recombination between electron and zinc interstitials and hole in the valence band. High intensity emission bands are observed at 458, 484, 524 and 598 nm. Peak at 458 corresponds to blue emission, where electron transition takes place from conduction band to the zinc interstitial sites through non-radiative process and then to the zinc vacancies. Green emission peak at 524 nm is due to singly ionized oxygen vacancy **[35-37]**. Where, electron transition takes place from zinc interstitials to oxygen vacancy. It is observed form **Fig. 6 (C)** that PL intensity of doped ZnO samples is much less as compared to pure ZnO. PL results shows that impurity doping can overcome the recombination between photogenerated holes and electrons, which is beneficial for photocatalytic reaction. It can be seen that C and N co-doped ZnO exhibit a lower intensity PL peak as compared to pure ZnO. Doping may offer competitive pathways for recombination resulting quenching of the broad green–orange emission. Photocatalytic activity of C, N co-doped ZnO prepared at 300 °C could enhance due to inhibition of electron-hole recombination.

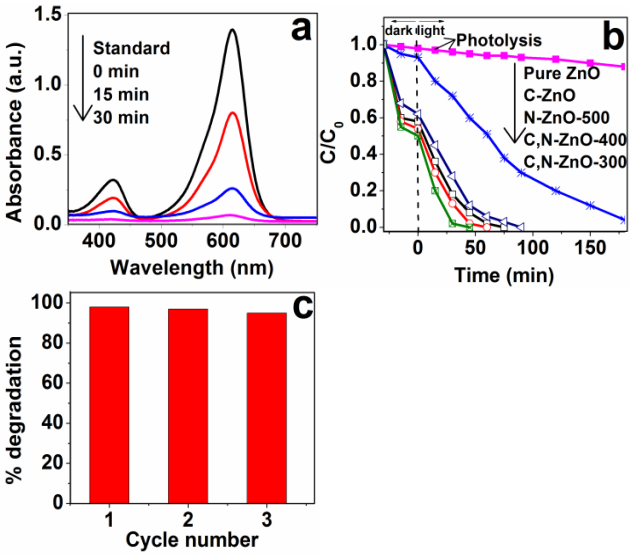

Fig. 7. (a) UV-visible spectra of MG solution irradiated with visible light at different time intervals in presence of C, N co-doped ZnO photocatalyst prepared at 300 °C, **(b)** photocatalytic performance of pure and doped ZnO **(c)** reuse of C, N co-doped ZnO photocatalyst prepared at 300 °C.

Visible light photocatalytic activity study

Visible light photocatalytic degradation of MG dye was investigated in presence of nanosized pure and doped ZnO. UV visible spectra of aqueous solution of MG irradiated with visible light at different time intervals in presence of C, N co-doped ZnO (obtained at 300 °C) were recorded and are presented in **Fig. 7(a)**. These Spectra shows characteristic peak maxima at 616 nm. As irradiation time increases the height of peak maxima at 616 nm decreases indicating photocatalytic degradation of MG. UV-visible spectra of the MG solution irradiated for different time intervals were recorded and amount of MG degraded was calculated. Plot of concentration of MG as a function of irradiation time in presence of different catalyst is presented in **Fig. 7(b)**. This figure show that solution kept in dark for 30 min in presence of catalyst calcined at different temperatures exhibit totally different behavior. Adsorption efficiencies of photocatalyst calcined at 300, 400 and 500 °C are 50.3, 45.6 and 38.1 % respectively. The adsorption efficiency of the dye increases with increasing the C content. In absence of catalyst no appreciable degradation of MG is observed even up to 180min, which means MG is fairly stable to visible-light irradiation. Photodegradation efficiency of ZnO decreases with increasing the calcination temperature of catalyst. As the calcination temperature increases C content in ZnO decreases. Catalyst calcined at 300 °C gives better photocatalytic activity, reaching ~98 % within 30min. The catalyst calcined at 400 and 500 °C degrades 87 and 72 % MG within 30 min. This can be due to difference in size and shape as well as C and N content doped on ZnO at different temperatures. For practical applications stability of photo catalyst during photodegradation is a vital factor.

C, N co-doped ZnO prepared at 300 ^{o}C exhibit better photocatalytic activity, therefore its stability was studied. Stability tests were performed by repeating the reaction three times using recovered photocatalyst. The data obtained is presented in **Fig. 7(c)**. This figure reveals that there is no noticeable decrease in photocatalytic activity up to third cycle. Which indicates that C, N co-doped ZnO prepared in the present work is highly stable and reusable photocatalyst.

Conclusion

Pure, C doped, N doped and C, N co-doped ZnO nanoparticles were prepared using microemulsion method. Optical studies show that due to substitution of oxygen in ZnO with C and N, band gap shifts from UV to visible region (3.08 to 2.16 eV). C, N co-doped ZnO prepared at 300°C shows lowest PL intensity of emission peaks which indicate that electron and hole pair recombination rate is inhibited and thus improves photocatalytic activity. Photocatalytic degradation efficiency of C, N co-doped ZnO for degradation of MG in aqueous solution is better than pure, C doped and N doped ZnO. Catalyst is highly stable it could be recycled and reused.

Acknowledgements

Authors are thankful to SAIF, IIT, Mumbai for recording the FE-SEM and EDX spectra of samples. One of the authors (Atul B. Lavand) is grateful to UGC, New Delhi, India for providing BSR-Research fellowship.

Author Contributions

AB - Performed the expeirments, YS - Data analysis, Wrote the paper.
It is declared that Authors have no competing financial interests.

Reference

1. Greene, L.E.; Law, M.; Goldberger, J.; Kim, F.; Johnson, J.C.; Zang, Y.; *Angew. Chem. Int. Ed.* **2003**, *42*, 3031. **DOI:** 10.1002/anie.200351461
2. Borkar, P.; Salker, A.V.; *Mater. Sci Eng. B.*, **2006**, *133*, 55. **DOI:** 10.1016/j.mseb.2006.05.007
3. Chen, C.C.; Lu, C.S.; Chung, Y.C.; Jan, J.L.; *J. Hazard. Mat*., **2007**, *141*, 520. **DOI:** 10.1016/j.jhazmat.2006.07.011
4. Singh, A.K.; Nakate, U.T.; *J. Nanoparticles*., **2013**, 310809, 1. **DOI:** 10.1155/2013/310809
5. Kazuhiko, M.; Kazunari, D.; *J. Phys. Chem. Lett*., **2010**, *1*, 2655. **DOI:** 10.1021/jz1007966
6. Saber, A.; Rasul, M.G.; Brown, R.; Hashib, M. A.; *J. Environ. Manag.*, **2011**, *92*, 311. **DOI:** 10.1016/j.jenvman.2010.08.028
7. Liu, G.; Wu, T.; Zhao, J.; Hidaka, H.; Serpone, N.; *Environ. Sci. Technol*., **1999**, *33*, 2081. **DOI:** 10.1021/es9807643
8. Zhao, J.; Wu, T.; Wu, K.; Oikawa, K.; Hidaka, H.; Serpone, N.; *Environ. Sci. Technol*., **1998**, *32*, 2394. **DOI:** 10.1021/es9707926
9. Hoffmann, M.R.; Martin, S.T.; Choi, W.; Bahnemann, D.W.; *Chem. Rev.*, **1995**, *95*, 69. **DOI:** 10.1021/cr00033a004
10. Konstantinou, I.K.; Albanis, T.A.; *Appl. Catal. B: Environ*., **2003**, *42*, 319. **DOI:** 10.1016/S0926-3373(02)00266-7
11. Muthirulan, P.; Devi, C. K. N.; Sundaram, M. M.; *Adv. Mater. Lett.*, **2014**, *5*, 163. **DOI:** 10.5185/amlett.2013.7507
12. Lavand, A. B.; Malghe Y. S.; *Adv. Mater. Lett.*, **2015**, *6*, 695. **DOI:** 10.5185/amlett.2015.5800
13. Daneshvar, N.; Salari, D.; Khataee, A. R.; *J. Photochem. Photobiol. A: Chem.*, **2004**, *162*, 317. **DOI:** 10.1016/S1010-6030(03)00378-2
14. Liu, Z.; Zhang, Q.; Li, Y.; Wang, H.; *J. Phys. Chem. Solids*., **2012**, *73*, 651. **DOI:** 10.1016/j.jpcs.2012.01.003
15. Bai, X.; Wang, L.; Zong, R.; Lv, Y.; Sun, Y.; Zhu, Y.; *Langmuir.*, **2013**, *29*, 3097. **DOI:** 10.1021/la4001768
16. Maiti, U. N.; Ahmed, S. F.; Mitra, M. K.; Chattopadhyay, K. K.; *Mater. Res. Bull*., **2009**, *44*, 134. **DOI:** 10.1016/j.materresbull.2008.03.019
17. Sakthivel, S.; Neppolian, B.; Shankar, M.V.; Arabindoo, B.; Palanichamy, M.; Murugesan, V.; *Sol. Energy. Mater. Sol. Cells.*, **2003**, *77*, 65. **DOI:** 10.1016/S0927-0248(02)00255-6
18. Kuriakose, S.; Satpati, B.; Mohapatra, S.; *Adv. Mater. Lett*., **2015**, *6*, 217. **DOI:** 10.5185/amlett.201 5.5693
19. Zhengrong, T.; James, V.; Jun, L.; Bonnie, M.; Matthew, M.; Mark, R.; Hiromi, K.; Huifang, X.; *Nature Mater*., **2003**, *2*, 821. **DOI:** 10.1038/nmat1014
20. Kumar, V.; Som, S.; Kumar, V.; Kumar, V.; Ntwaeaborwa, O.; Coetseea, E.; Swart, H.; *Chem. Eng. J*.; **2014**, *255*, 541. **DOI:** 10.1016/j.cej.2014.06.027
21. Kumar, V.; Kumar, V.; Som, S.; Purohit, L.; Ntwaeaborwa, O.; Swart, H.; *J. Alloys Comp*.; **2014**, *594*, 32. **DOI:** 10.1016/j.jallcom.2014.01.110
22. Kumar, V.; Swart, H.; Gohain, M.; Kumar, V.; Soma, S.; Bezuindenhoudt, B.; Ntwaeaborw, O.; *Ultrasonics Sonochem*.; **2014**, *21*, 1549. **DOI:** 10.1016/j.ultsonch.2014.01.019
23. Lavand, A.B.; Malghe, Y. S.; *Int. J. Photocatal.*, **2015**, 790153, 1. **DOI:** 10.1155/2015/790153
24. Qin, H.; Li, W.; Xia, Y.; He, T.; *Appl. Mater. Interfaces*.; **2011**, *3*, 3152. **DOI:** 10.1021/am200655h
25. Vo, V.; Thi, T. P.T.; Kim, H.Y.; Kim, S. J.; *J. Phys. Chem Solids*., **2014**, *75*, 403. **DOI:** 10.1016/j.jpcs.2013.11.011
26. Flores, N. M.; Pal, U.; Galeazzi, R.; Sandoval, A.; *RSC. Adv*., **2014**, *4*, 41099. **DOI:** 10.1039/c4ra04522j
27. Jimenez-Gonzalez, A. E.; Urueta, J. A. S.; Suarez-Parra, R.; *J. Cryst. Growth*., **1998**, *192*, 430. **DOI:** 10.1016/S0022-0248(98)00422-9
28. Jinfeng, L.; Qiwu, Z.; Jun, W.; Fumio, S.; Masashi, U.; *Powder Technol*., **2006**, *162*, 33. **DOI:** 10.1016/j.powtec.2005.12.007
29. Hong, R.Y.; Li, J. H.; Chen, L. L.; Liu, D. Q.; Li, H. Z.; Zheng, Y.; Ding, J.; *Powder Technol*. **2009**, *189*, 426. **DOI:** 10.1016/j.powtec.2008.07.004
30. Zou, C.W.; Yan, X.D.; Han, J.; Chen, R.Q.; Gao, W.; Metson, J.; *Appl. Phys. Lett*., **2009**, *94*, 171903. **DOI:** 10.1063/1.3125255
31. Suryanarayana, C.; Nortan, M. G.; X-ray Diffraction: A practical Approach; *Plenum Publishing Corporation*: *New York*, **1998**. **DOI:** 10.1007/978-1 -4899-0148-4
32. Oxley, J.; Smith, J.; Naik, S.; Moran, J.; *J. Energ. Mater*., **2009**, *27*, 17. **DOI:** 10.1080/07370650802328814
33. Nakamura, R.; Tanaka, T.; Nakato, Y.; *J. Phys. Chem. B*. **2004**, *108*, 10617. **DOI:** 10.1021/jp048112q
34. Bhirud, A.; Sathaye, S.; Waichal, R.; Nikam, L.; Kale, B. *Green Chem*. **2012**, *14*, 2790. **DOI:** 10.1039/C2GC35519A
35. Vasile, O-R; Andronescu, E; Ghitulica, C; Vasile, B, S; Opera, O; Vasile, E; Trusca, R.; *J. Nanopart. Res*., **2012**, *14*, 1269. **DOI:** 10.1007/s11051 -012-1269-7
36. Samanta, P. K; Bandyopadhyay, A. K.; *Appl. Nanosci*., **2012**, *2*, 111. **DOI:** 10.1007/s13204-011 -0038-8
37. Kumar, V.; Kumari, S.; Kumar, P.; Kar, M.; Kumar, M., *Adv. Mater. Lett*., **2015**, *6*, 139. **DOI:** 10.5185/amlett.201 5.5632

Supporting Information

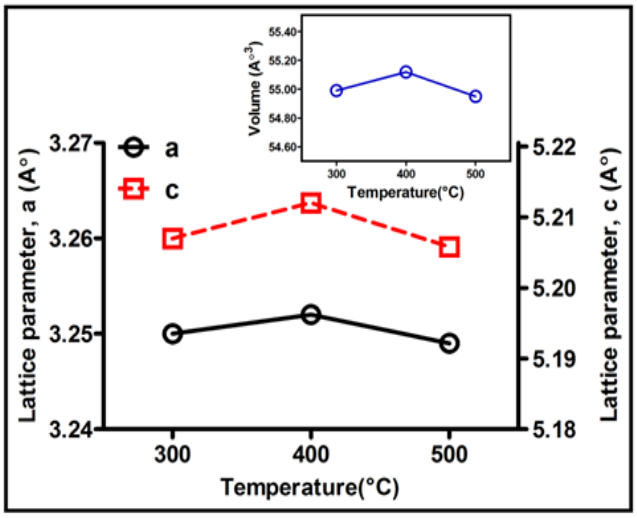

Fig. S1. Variation of lattice parameters with respect to temperature.

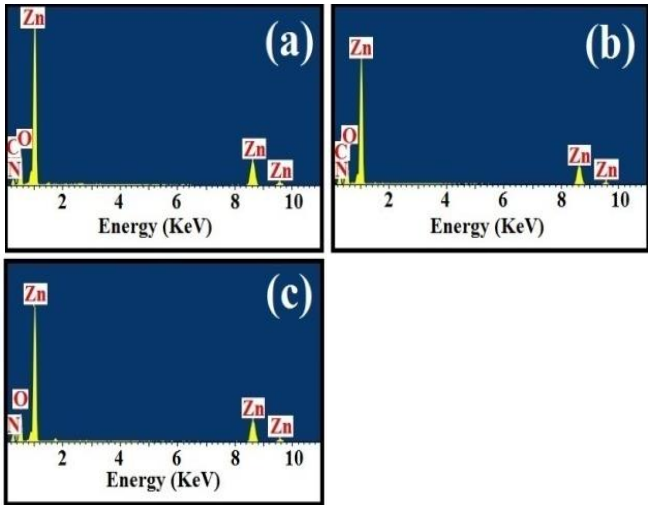

Fig. S2. EDX spectra of precursor calcined at (a) 300 (b) 400 and (c) 500 °C.

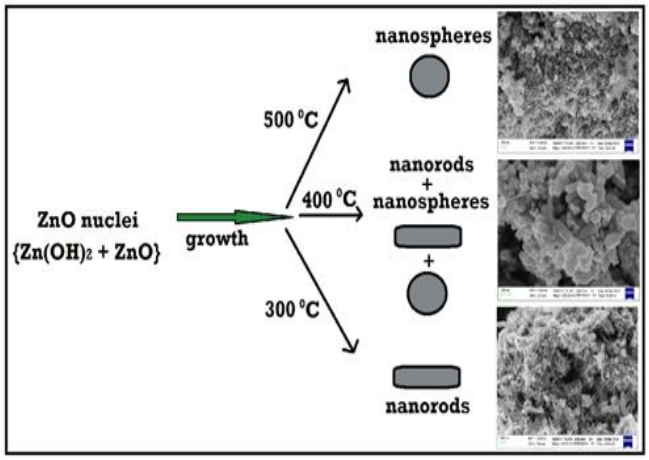

Fig. S3. Growth mechanism of C/N doped ZnO.

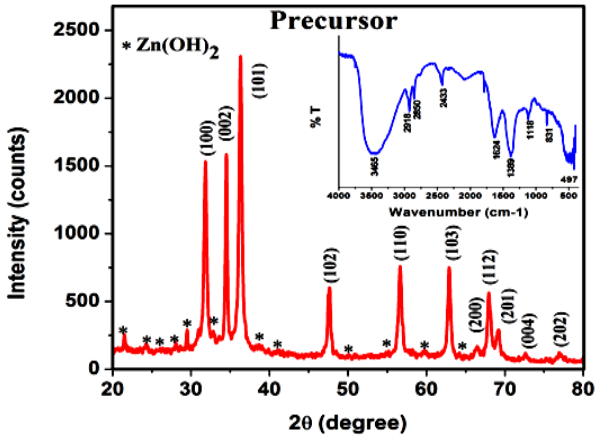

Fig. S4. XRD pattern and inset shows FTIR spectra of N doped ZnO precursor.